Modelling and measurement of mercury transport through ceramic membranes

Sande, van de, M.J.

Award date:
1997

MODELLING AND MEASUREMENT OF MERCURY TRANSPORT THROUGH CERAMIC MEMBRANES

By Marco van de Sande

VDF/NG 97-06

Please note:

Due to the confidential nature of the research done at Philips Lighting, this report is not a complete reflection of my graduation project. Some parts of the original paper have been shortened, whereas some other parts are completely omitted.

TECHNOLOGY ASSESSMENT

In low pressure discharge lamps it is important that the processes of mercury diffusion are well understood, in order to guarantee an efficient use and long lifetime. There is also interest in the diffusion processes of mercury in porous materials. The goal of this investigation is to build a measurement system that can determine the diffusion rates of mercury through porous membranes and to study the temperature dependence of the diffusion of mercury through a microporous SiO_2 membrane on an Al_2O_3 support.

The diffusion rates are determined by monitoring changes in the mercury pressure in an optical cuvette containing a mercury tap upon temperature steps. The mercury pressure is measured in a transmission measurement. The membranes for which the diffusion rate is measured are a macroporous α-Al_2O_3 membrane (the substrate), a mesoporous γ-Al_2O_3 membrane on an α-Al_2O_3 substrate and a microporous SiO_2 membrane on top of the α/γ-Al_2O_3 membrane.

One of the most important conclusions is that mercury pressures can be measured with an uncertainty of less than 20% for pressures between 0.2 and 4 Pa. Furthermore, the transport through the microporous membrane is activated. The diffusion mechanism in the SiO_2 membrane is micropore diffusion. The temperature dependence of this type of transport is described with an activation energy E_a, which is in the order of -5 kJ/mol for the SiO_2 membranes used. The fact that E_a is negative, leads to a negative temperature dependence of the transport.

TABLE OF CONTENTS

TECHNOLOGY ASSESSMENT ii

TABLE OF CONTENTS iii

1 INTRODUCTION 1
1.1 General description of low pressure discharge lamps 1
1.2 Mercury pressure control in discharge lamps 1
1.2.1 Liquid mercury 2
1.2.2 Amalgams 2
1.2.3 Mercury dynamics 4
1.3 Scope of this report 5

2 TRANSPORT THROUGH CERAMIC MEMBRANES 6
2.1 Introduction 6
2.2 Gas transport through macro- and mesoporous membranes 7
2.2.1 Viscous flow 8
2.2.2 Knudsen diffusion 8
2.2.3 Transition flow 9
2.2.4 Surface diffusion 9
2.3 Gas transport in microporous membranes 10
2.3.1 Steady flow within a microporous membrane 11
2.3.2 Interface processes 12
2.3.3 Adsorption isotherms 13
2.3.4 The diffusion equation 14

3 EXPERIMENTAL SETUP AND MEASUREMENTS 16
3.1 Experimental setup for mercury pressure measurements 16
3.1.1 The hardware 16
3.1.2 Calibration of the experimental setup 17
3.2 Determination of diffusion coefficients 18

4 RESULTS 23
4.1 Calibration and amalgam measurements 23
4.2 Measurements on ceramic membranes 26
4.2.1 Verification of the measurement technique 26
4.2.2 Transport types, transport rates and activation energies . 29
4.2.3 Concluding remarks 35

5 CONCLUSIONS 36

REFERENCES 38

LIST OF SYMBOLS 39

ACKNOWLEDGMENTS 41

1 INTRODUCTION

1.1 General description of low pressure discharge lamps

In low pressure discharge lamps, like TL and CFL lamps, mercury atoms are excited by collisions with electrons going from one electrode to the other, accelerated by the electric field between the electrodes. When the mercury atoms fall back to the ground state ultraviolet radiation is emitted. A fluorescent powder on the inside of the glass tube converts this radiation into visible light. This principle is illustrated in figure 1.1.

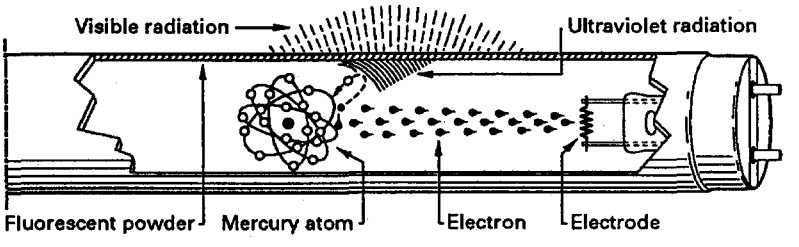

Figure 1.1 The working principle of a low pressure discharge lamp (TL lamp).

An important parameter in these lamps is the density of mercury atoms or the mercury vapour pressure. If the mercury pressure is too low the probability of collisions between mercury atoms and electrons is too low and thus the light output is low. However, if the mercury pressure is too high, mercury atoms in the ground state will reabsorb the UV radiation. This leads to an increase in the number of excited atoms. As a consequence, there is an increase in the probability of interactions in which the excited mercury atom loses (part of) its energy without radiation. Again the light output is low. In other words, there is an optimal mercury pressure for which the light output is at a maximum. For standard lamps this pressure is in the order of 1 Pa.

1.2 Mercury pressure control in discharge lamps

In low pressure discharge lamps working with mercury there is mercury consumption, caused by absorption of mercury in the emitter and in the fluorescent powder. This is typically in the order of milligrams in the course of the lifetime. Therefore, if exactly enough mercury is dosed for maximum light output (usually 5 to 100 μg, depending on the lamp type), the amount of mercury will significantly decrease within 100 hours, causing the

light output to decrease. Hence the lifetime of a so-called unsaturated lamp would be far shorter than the typical lifetime of a TL lamp (approximately 8000-10000 hours).

1.2.1 Liquid mercury

A solution to this problem is the saturated lamp. In these lamps enough mercury is supplied for a much longer lifetime. The mercury pressure, which equals the saturated mercury vapour pressure, depends on the temperature of the coldest spot in the discharge vessel.

The temperature trajectory in which the mercury pressure is such that the light output is higher than 90% of the maximum light output is called ΔT_{90}. The optimum temperature for TL lamps is approximately 45°C and ΔT_{90} is approximately 30°C. Figure 1.2 shows the light output as a function of the temperature.

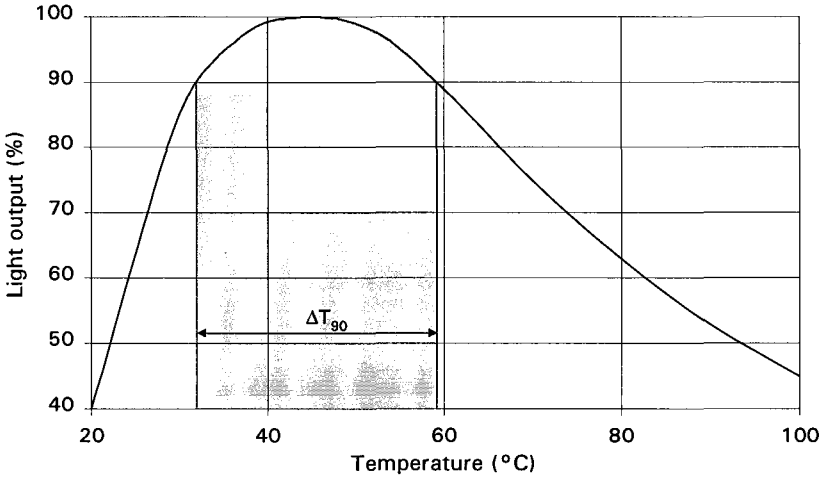

Figure 1.2 Light output as a function of temperature (schematically).

When the lamp is off, it is at the ambient temperature (25°C), so the mercury pressure is lower than the optimal pressure. The light output directly after ignition (Initial Light Output, ILO) is therefore low (approximately 50%). When the lamp gets warmer, the mercury pressure increases. Then the light output also increases (as long as the optimum pressure is not yet reached). The runup time is defined to be the time before the lamp reaches 80% light output. For discharge lamps with liquid mercury this is typically in the order of a few minutes.

1.2.2 Amalgams

The further miniaturization and operation at higher currents of TL and CFL lamps causes the temperature of these lamps to increase. A forced cold spot can be created in order to keep the mercury pressure at its optimum. This is done in the PLC lamps.

Another solution is the application of amalgams. An amalgam is an alloy of mercury and one or more other metals. At a given temperature, the saturated mercury pressure of a lamp amalgam is much lower than that of pure mercury. The optimum mercury pressure is therefore reached only at much higher temperatures (80-100°C). Moreover, ΔT_{90} is generally broader for amalgams. For the $Pb_{20}Bi_{46}Sn_{34}$ amalgam containing 3 wt% of mercury[1], this is illustrated in figure 1.3.

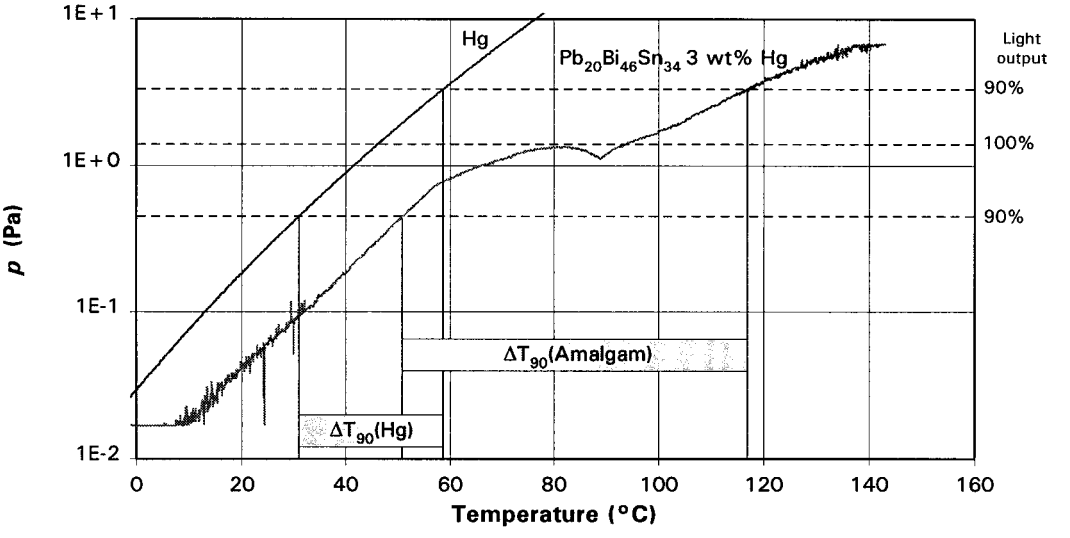

Figure 1.3 The mercury pressure of pure mercury and that of the $Pb_{20}Bi_{46}Sn_{34}$ 3 wt% Hg amalgam as a function of the temperature. Evidently ΔT_{90} is broader and at a higher temperature for the amalgam.

A major drawback of the application of amalgams in TL/CFL lamps is the relative low ILO and slow runup. The problem is that the amalgam absorbs almost all mercury in the lamp at lower temperatures when the lamp is off. Auxiliary amalgams can be used to improve the runup. Auxiliary amalgams are small amounts of amalgam (different from the main amalgam) close to the electrodes of the lamp (see figure 1.4). Therefore, upon ignition of the lamp, the electrodes heat the auxiliary amalgams quickly, which causes the mercury in the auxiliary amalgam to evaporate almost immediately. The lamp is at 100% light output shortly after ignition. The runup of these lamps is often even faster than that for mercury lamps. However, an auxiliary amalgam must have a lower mercury pressure than the main amalgam, otherwise, the auxiliary amalgam would not take up enough mercury. Because of this lower mercury pressure, the ILO decreases even further. Moreover, when the lamp is switched on, an auxiliary amalgam often leads to an excess in mercury pressure, which causes the light output to decrease temporarily. Only when the main amalgam is at high temperature the light output is stable close to 100% light output.

---

1. This amalgam will be denoted as $Pb_{20}Bi_{46}Sn_{34}$ 3 wt% Hg. This means that the amalgam contains 3 wt% mercury and the alloy without mercury contains 20 wt% lead, 46 wt% bismuth and 34 wt% tin, so all fractions are denoted in wt%. In Philips nomenclature the term "direct amalgam" is often used for amalgams, while the alloy without mercury is called "amalgam".

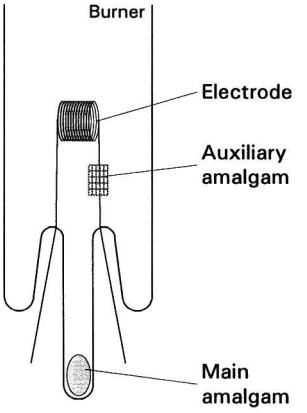

Figure 1.4 Schematic illustration of an auxiliary amalgam in a TL lamp.

1.2.3 Mercury dynamics

The behaviour of an amalgam lamp is influenced by diffusion processes of mercury in various materials and wall effects (absorption). Therefore it is of great importance that the interaction between mercury and other materials is elaborately investigated. In the present investigation, diffusion processes of mercury in microporous SiO_2 modified ceramic membranes are studied. The ceramic membrane is a layered structure. It consists of an α-Al_2O_3 substrate with an γ-Al_2O_3 and SiO_2 layer. The α-Al_2O_3 substrate is macroporous (pores wider than 50 nm), whereas the γ-Al_2O_3 layer is mesoporous (pores-sizes between 2 and 50 nm). The silica (SiO_2) layer is the only microporous layer (pores narrower than 2 nm). The Al_2O_3 layers merely serve as a support. In figure 1.5 a picture of this membrane is shown.

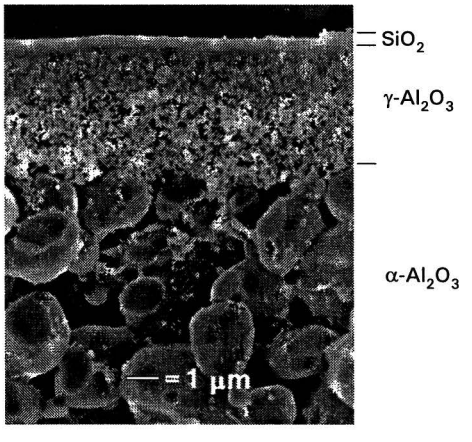

Figure 1.5 Schematic illustration of the microporous membrane considered in this investigation.

1.3 Scope of this report

A theory about the mercury transport in ceramic porous membranes is presented in chapter 2. Especially the temperature dependence of the transport is given attention. Chapter 3 is concerned with the experimental setup for the measurement of mercury pressures and mercury fluxes through a membrane. In chapter 4 the results of the measurements that have been performed will be presented. This concerns both measurements of the saturated mercury pressure of amalgams and measurements of diffusivities of mercury in the ceramic membranes. Conclusions from this investigation are given in chapter 5.

2 TRANSPORT THROUGH CERAMIC MEMBRANES

2.1 Introduction

For a description of mercury transport through ceramic membranes generally Fick's law is used:

$$\vec{J} = -D\vec{\nabla}n, \tag{2.1}$$

where $\vec{J}$ is the flux (mol/m^{2}s), n is the concentration (mol/m^3) and D is the Fickian diffusion coefficient (m^2/s). Originally this equation was intended to describe diffusion, but also for other types of transport (even viscous flow, see below) a coefficient D can be found so that the flux obeys (2.1).

Although the real pore structure in a ceramic membrane generally consists of a more or less random network of interconnecting pores of varying diameter and orientation, it is helpful to approximate the pores by straight cylindrical pores. A factor to account for this approximation is the tortuosity τ:

$$\tau \equiv L/d, \tag{2.2}$$

where L is the effective length of a pore and d is the length measured along the membrane, equal to the thickness of the membrane. The tortuosity is a measure for the complexity of the structure. Another important parameter is the porosity,

$$\varepsilon \equiv \frac{\rho_{th} - \rho}{\rho_{th}}, \text{ or } \varepsilon \equiv A_E/A, \tag{2.3}$$

where ρ is the mass density of the material (kg/m^3), ρ_{th} is the theoretical density (for a massive membrane), A_E is the effective surface for diffusion (the pore surface) and A is the total surface of the membrane. Thus if $\varepsilon = 0.1$ the mass is 10% lower than expected and the pores cover 10% of the total surface. The factors ε and τ will emerge in almost all equations describing diffusion in porous materials.

Furthermore membranes are said to be macroporous if they contain pores with a diameter (pore size) of 50 nm or more. Mesoporous membranes have pore sizes between 2 and 50 nm and microporous membranes have pores narrower than 2 nm.

2.2 Gas transport through macro- and mesoporous membranes

An important parameter in macro- and mesoporous membranes is the Knudsen number of the gas in the pores:

$$\mathrm{Kn} \equiv \frac{\lambda}{d_p}. \tag{2.4}$$

Here λ is the mean free path length of the gas molecules and d_p is the diameter of the pores (pore size). For a single gas λ is given by [4]:

$$\lambda = \frac{1}{\sqrt{2}\pi\sigma^2 n}, \tag{2.5}$$

where $\pi\sigma^2$ is the cross section for collisions. In a lamp, however, there is usually a mixture of two (or sometimes more) gases, one of which is mercury. The concentration of mercury is then much lower than the concentration of the background gases, so the mercury atoms can be assumed to collide only with the background gas molecules. If there is only one background gas, the mean free path length of the mercury atoms generalizes to

$$\lambda = \left(\frac{g}{v}\pi\sigma^2 n\right)^{-1}. \tag{2.6}$$

Now for the concentration n both the mercury and the background gas are considered and for σ the average value of σ of both different molecules is used. The velocity of the mercury atoms is v and g is a factor containing the velocities v and v_b, the velocity of the background gas:

$$g = (v^2 + v_b^2)^{\frac{1}{2}}. \tag{2.7}$$

If M is the molecular mass of mercury and M_b is the molecular mass of the background gas molecules, g/v equals

$$\frac{g}{v} = \left(1 + \frac{v_b^2}{v^2}\right)^{\frac{1}{2}} = \left(1 + \frac{kT/M_b}{kT/M}\right)^{\frac{1}{2}} = \left(1 + \frac{M}{M_b}\right)^{\frac{1}{2}}. \tag{2.8}$$

For mercury in an argon background gas, the factor g/v equals

$$\frac{g}{v} = \left(1 + \frac{M_{Hg}}{M_{Ar}}\right)^{\frac{1}{2}} = 2.455. \tag{2.9}$$

The cross section for collisions is $\pi\sigma_{Hg,Ar}^2$, where

$$\sigma_{Hg,Ar} = \frac{\sigma_{Hg} + \sigma_{Ar}}{2} = 0.312\ \mathrm{nm}. \tag{2.10}$$

At a temperature $T = 298$ K and a pressure $p = 400$ Pa, the density of atoms is $n = p/kT$, where k is the Boltzmann constant, and thus $n = 9.72 \cdot 10^{22}$. Then the mean free path length λ follows from (2.6):

$$\lambda = 13.7\ \mu\mathrm{m}. \tag{2.11}$$

The type of transport through the pores depends on the Knudsen number (2.4). For low Knudsen numbers ($Kn \ll 1$) collisions of the atoms with other atoms or molecules dominate collisions with the pore wall and the transport type is viscous flow. If $Kn \gg 1$ mercury atoms collide mainly with the pore wall and "do not see" the other atoms. The gas is then said to be a Knudsen gas and the transport is Knudsen diffusion. If $Kn \approx 1$ the transport mechanism is something in between Knudsen diffusion and viscous flow, which is called transition flow or slip flow.

2.2.1 Viscous flow

For small Knudsen numbers the transport type in the pores is viscous flow, or sometimes called convection. This occurs in broad pores (macroporous material; equation (2.4)) and at high pressures (high concentrations; equation (2.5) and (2.6)). In fact, viscous flow is a type of bulk diffusion. Another type of bulk diffusion is turbulent flow. For pure turbulent flow the velocity of the gas is independent of the location in the pore, but for laminar flow (viscous flow) the velocity of the gas depends on the distance to the pore wall, described by Poiseuille. In general, turbulent flow occurs for Reynolds numbers greater than 1. The Reynolds number is defined as

$$\mathrm{Re} \equiv \frac{\rho v d_p}{\eta},$$

where ρ is the mass density (kg/m^3) and η is the viscosity (Ns/m^2). In practice, $\mathrm{Re} \gg 1$ occurs only in pores with a size in the order of a micron. Therefore, turbulent flow is not expected in the ceramic membranes. Laminar flow is described by Poiseuille's equation. This formally equivalent to (2.1) with a diffusivity [11]

$$D_P = \frac{p d_p^2}{32\eta}, \tag{2.12}$$

where p is the pressure and d_p is the pore size. In real porous media this diffusion coefficient must be modified to account for the complexity of the structure (indicated by the tortuosity τ, equation (2.2)) and the effective surface, available for diffusion (indicated by the porosity ε, equation (2.3)):

$$D_P = \frac{\varepsilon}{\tau} \cdot \frac{p d_p^2}{32\eta}. \tag{2.13}$$

In principle, this equation is derived for single gases, but it is also valid in mixtures because viscous flow doesn't affect the concentration of the gases. The viscosity η, however, is affected by the composition of the mixture.

Since $\eta \sim \sqrt{T}$ and $p \sim T$ the temperature dependence of the diffusion coefficient is

$$D_P \sim \sqrt{T}. \tag{2.14}$$

2.2.2 Knudsen diffusion

If $Kn \gg 1$ the transport type in the pores is Knudsen diffusion. This occurs in narrow pores (mesoporous material; equation (2.4)) and at low pressures (low concentrations n; equa-

tion (2.5) and (2.6)). This type of transport is likely to occur in the porous membranes measured. Knudsen flow is described by the Knudsen equation. This is (2.1) with a diffusivity [11]

$$D_K = \frac{d_p}{3}\langle v \rangle = \frac{d_p}{3}\sqrt{\frac{8RT}{\pi M}}, \tag{2.15}$$

with $\langle v \rangle$ the average thermal velocity of the mercury atoms. R is the universal gas constant (8.31 $J \cdot mol^{-1}K^{-1}$) and M is the molecular mass of the mercury vapour (kg/mol). Also this equation has to be corrected with a factor ε/τ. Furthermore it is assumed that the molecules perfectly reflect on the pore wall. Usually, this is not the case, because the pore wall has a certain roughness which causes diffuse reflections. This effect is taken into account by introducing a reflection factor Θ_K, which equals unity in the case of perfect reflection, and is larger otherwise. With these modifications (2.15) becomes

$$D_K = \frac{d_p}{3}\frac{\varepsilon}{\tau\Theta_K}\sqrt{\frac{8RT}{\pi M}}. \tag{2.16}$$

Like with viscous flow, this equation is valid not only for single gases, but for mixtures as well. Here this is due to the fact that collisions between molecules are negligible compared to collisions with the pore wall. In mixtures, M is the weighted average of the molecular masses.

From equation (2.16) it is clear that D_K is proportional to $\sqrt{T}$.

2.2.3 Transition flow

For Knudsen numbers close to unity both Knudsen flow and viscous flow play a role. With laminar (Poiseuille) flow the velocity of the gas molecules is zero near the pore wall. With Knudsen diffusion, however, the speed of the molecules is equal everywhere in the pore. In the transition region the flow is dependent on the location in the pore, but the velocity of the gas is not zero near the pore wall. Therefore transition flow is sometimes called slip flow. The diffusivity D can be written as a combination of D_K and D_P. This will not be discussed in this report.

2.2.4 Surface diffusion

A form of diffusion that becomes more and more important for narrow pores is surface diffusion. For surface diffusion to occur, the mercury atoms have to be physisorbed by the pore wall. Physisorption is due to Van der Waals forces between the solid surface and the adsorbate atoms. Therefore, surface diffusion only plays a significant role, if the pore diameter is not very much larger than the range on which the Van der Waals force acts, which is in the order of the size of an atom. The occupation degree θ is defined as

$$\theta \equiv \frac{\#\text{ sites occupied}}{\#\text{ sites available}} = \frac{q}{q_s}, \tag{2.17}$$

where q is the concentration of the adsorbed atoms (mol/m^2) and q_s is the saturated adsorption (mol/m^2). Here it is assumed that only monolayer coverage occurs.

Surface diffusion is diffusion from one site on the surface to another. This can be described by the two-dimensional equivalent of Fick's law:

$$\vec{j}_s = -D_s \vec{\nabla} q, \tag{2.18}$$

where D_s is the surface diffusion coefficient (m^2/s) and $\vec{j}_s$ is the surface diffusion flux (mol/ms). The flux through a straight, cylindrical pore is then:

$$j_{pore} = \pi d_p \cdot -D_s \frac{dq}{dz}, \tag{2.19}$$

where z is the coordinate along in the pore in the direction of diffusion. With the definition of the porosity ε (equation (2.3)) and the surface of a single pore, $\pi {d_p}^2/4$, the number of pores per unit area on the porous material is $s = 4\varepsilon/\pi {d_p}^2$. Using the occupation degree θ (equation (2.17)), the flux (mol/m^2s) through the membrane due to surface diffusion becomes

$$J_s = s \cdot j_{pore} = -\frac{4\varepsilon}{\tau} \cdot \frac{D_s}{d_p} \cdot q_s \frac{d\theta}{dz}. \tag{2.20}$$

The factor $4\varepsilon/d_p$ is in fact the specific surface of the porous material (m^2/m^3), and the factor $1/\tau$ is introduced to account for the tortuosity.

As will become clear in the following section, the temperature dependence of D_s is

$$D_s \sim T \cdot \exp\left(-\frac{E_a}{RT}\right), \tag{2.21}$$

where E_a is an apparent activation energy for diffusion.

2.3 Gas transport in microporous membranes

For micropore diffusion a model proposed by Barrer is used [3]. The transport mechanism is very similar to surface diffusion. However, a micropore can be modelled by a channel with several sites and therefore micropore diffusion can be described by a one-dimensional Fick's law. The potential energy of an adsorbate atom as a function of z, the location along the pore, is schematically given in figure 2.1. This profile is caused by the Van der Waals interactions with the atoms of the ceramic membrane. Each location for which the potential energy is at a minimum is a site. The occupation degree θ_i is now the chance that an adsorbate atom occupies site i.

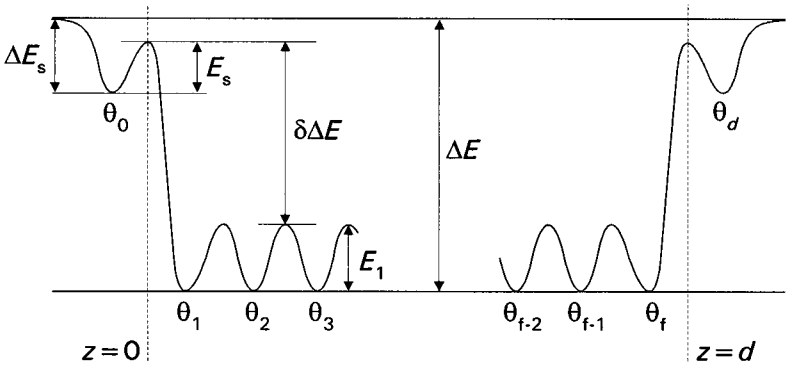

Figure 2.1 The potential energy of an adsorbate atom as a function of the location z in the micropore (schematically).

2.3.1 Steady flow within a microporous membrane

The steady-state flux of mercury in the pore can be derived from θ_i. For a mercury atom, the probability of jumping over the energy barrier E_1[1] to location i is:

$$P_i(E_1) = k_1 \exp\left(-\frac{E_1}{RT}\right) \cdot (1-\theta_i) , \tag{2.22}$$

thus the probability is proportional to an exponential factor containing the energy E_1 and to the (average) space that is left at the i-th site. The mercury flux in a pore from site i to site $i+1$ is then

$$\vec{j_i} = \theta_i \cdot P_{i+1}(E_1) = k_1 \theta_i (1-\theta_{i+1}) \exp\left(-\frac{E_1}{RT}\right) \tag{2.23}$$

and the mercury flux in a pore from site $i+1$ back to site i is

$$\overleftarrow{j_i} = \theta_{i+1} \cdot P_i(E_1) = k_1 \theta_{i+1} (1-\theta_i) \exp\left(-\frac{E_1}{RT}\right) . \tag{2.24}$$

The total mercury flux from site i to site $i+1$ is then

$$j_i = \vec{j_i} - \overleftarrow{j_i} = k_1 \exp\left(-\frac{E_1}{RT}\right) \cdot (\theta_i - \theta_{i+1}) . \tag{2.25}$$

This is of course equal to the total flux j in the pore: $j = j_i$. The occupation degrees θ_i, $2 \le i \le$ f-1 can be eliminated by adding the equations (2.25) for all i:

$$(\text{f-1})j = k_1 \exp\left(-\frac{E_1}{RT}\right) \cdot \sum_{i=1}^{\text{f-1}} (\theta_i - \theta_{i+1}) = k_1 \exp\left(-\frac{E_1}{RT}\right) \cdot (\theta_1 - \theta_f) . \tag{2.26}$$

If there are s pores per unit cross-section area normal to the direction of j the total flux J_{id} due to diffusion in the micropore is:

$$J_{id} = sj = \frac{sk_1}{\text{f}-1} \exp\left(-\frac{E_1}{RT}\right) \cdot (\theta_1 - \theta_f) . \tag{2.27}$$

The energy E_1 is called the activation energy for diffusion.

---

1. All energies are in J/mol.

2.3.2 Interface processes

The flow in the pores is now known for given occupations degrees θ_1 and θ_f. However, these occupation degrees are steady-state rather than equilibrium ones, since there is a pressure difference across the membrane and thus there is diffusion. Only the equilibrium occupation degrees can be calculated from a given pressure (see section 2.3.3). Therefore, the flow is to be expressed in the equilibrium occupations.

Moreover, entry into and exit from the porous crystals can occur only through the mouths of the channels. Therefore interface processes that involve the channel mouth should also be considered. For transport through a porous crystal there are a few different steps:

1. Adsorption from the gas phase onto site 0′ on the surface of the porous membrane and migration to site 0 near the pore mouth (flux $F_2 \cdot J$ in figure 2.2).
2. Adsorption from the gas phase onto site 0 near the pore mouth on the membrane (flux $F_1 \cdot J$).
3. Migration from site 0 near the pore mouth to site 1, the first site in the micropore (flux $J = F_1 J + F_2 J$; $F_1 + F_2 = 1$).
4. Micropore diffusion in the pores from site 1 to site f (J_{id}).
5. Desorption from the last site f in the pore to the external surface (site d).
6. Desorption from the external surface (site d) to the gas phase or migration to site d′ followed by desorption to the gas phase.

The potential energy of the atoms at the *i*-th site is shown in figure 2.1.

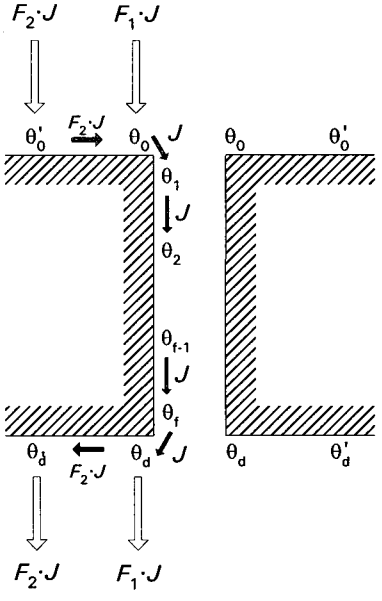

Figure 2.2 Schematic representation of the interface processes and fluxes involved in micropore diffusion.

An extensive calculation (done by Barrer, see [3]) of adsorption and desorption rates to and from the different sites for a given potential energy curve (figure 2.1), shows that the ratio of the intercrystalline flux J_{id} and total flux J can be expressed in terms of the equilibrium occupation degrees (indicated by the subscript ,eq):

$$\frac{J_{id}}{J} = 1 + \left(\frac{1-\theta_{1,eq}}{1-\theta_{0,eq}} + \frac{1-\theta_{f,eq}}{1-\theta_{d,eq}} \right) \frac{\exp(\delta\Delta E/RT)}{f-1}, \tag{2.28}$$

with J_{id} given by equation (2.27), but with θ_1 and θ_f replaced by their equilibrium values $\theta_{1,eq}$ and $\theta_{f,eq}$ respectively, and

$$\delta\Delta E \equiv E_s + \Delta E - \Delta E_s - E_1 . \tag{2.29}$$

In the derivation of (2.28) it is assumed that the pre-exponential constant k_1 in (2.22) equals the pre-exponential constant k_a in the jumping probabilities between sites 0 and 1 and sites f and d. This is linked with the assumption that the potential energy wells involving k_1 and k_a have similar contours near their minima. Furthermore the occupation degrees at the surface, θ_0, θ_0', θ_d and θ_d' are assumed to equal their equilibrium values. This assumption is justified by the fact that the adsorption from the gas phase onto the surface and desorption from the surface to the gas phase are much faster processed than the micropore diffusion itself.

For large f, thus if there are many adsorption sites along the pore, the factor (f-1) approaches d/d_j, where d_j is the jump distance and d is the thickness of the membrane. If both the internal and the external sorption isotherms obey Henry's law, thus all occupation degrees are very small ($\theta_i \ll 1$, see section 2.3.3), then equation (2.28) can be rewritten as:

$$\frac{J_{id}}{J} = 1 + 2\frac{d_j}{d}\exp\left(\frac{\delta\Delta E}{RT}\right) \equiv C_{int}, \tag{2.30}$$

thus from (2.27) it follows that

$$J = \frac{sk_1}{C_{int}} \cdot \frac{d_j}{d}\exp\left(-\frac{E_1}{RT}\right) \cdot (\theta_{1,eq} - \theta_{f,eq}) . \tag{2.31}$$

Here the factor f-1 is again replaced by d/d_j and the occupation degrees θ_1 and θ_f are replaced by their equilibrium values.

2.3.3 Adsorption isotherms

The occupation degrees $\theta_{1,eq}$ and $\theta_{f,eq}$ for given temperature T and pressure p can be approximated by an adsorption isotherm. One of the simplest adsorption isotherms is Langmuir's isotherm. This is a good approximation, provided that the following assumptions are valid:

- There is only monolayer coverage, as can be assumed to be the case in very narrow pores and at low pressures.
- There is no interaction between adsorbed atoms. This is not the case for very high occupation degrees ($\theta > 0.75$) but this is not the case on a ceramic membrane used for exeriments used in this report. This assumption leads to a diffusivity that is independent of the occupation degree θ.
- The adsorption surface is uniform.

The reaction that forms an equilibrium is A(g) + M(surface) $\rightleftarrows$ AM(surface), where A is the adsorbent and M is the adsorber. The reaction rates are k_a ($s^{-1}Pa^{-1}$) and k_d (s^{-1}) for ad-

sorption and desorption respectively. If there are N sites per unit area, the number of adsorbed atoms changes with:

$$N\frac{d\theta}{dt} = N\frac{d\theta}{dt}\bigg|_{adsorption} + N\frac{d\theta}{dt}\bigg|_{desorption} = k_a p N(1-\theta) - k_d N\theta . \tag{2.32}$$

In equilibrium the occupation degree is constant, so from (2.32) it follows that

$$k_a p\,(1-\theta_{eq}) = k_d \theta_{eq} \tag{2.33}$$

or

$$\theta_{eq} = \frac{Kp}{1+Kp}, \text{ where } K \equiv \frac{k_a}{k_d}. \tag{2.34}$$

For low occupation degrees this equation simplifies even further to Henry's Law:

$$\theta_{eq} = Kp . \tag{2.35}$$

The constant K is then called Henry's constant.

Since K is an equilibrium constant, for the temperature dependence of K the Van 't Hoff equation holds:

$$\frac{\Delta H_{ads}}{RT^2} = \left(\frac{\partial}{\partial T}\ln K\right)_\theta , \tag{2.36}$$

where ΔH_{ads} is the energy that is needed when an atom is adsorbed. So $\Delta H_{ads} = -q_{st}$, where q_{st} is the isosteric heat of adsorption (which is released upon adsorption). The Henry constant becomes

$$K = K_0 \exp\left(-\frac{\Delta H_{ads}}{RT}\right) = K_0 \exp\left(\frac{q_{st}}{RT}\right). \tag{2.37}$$

2.3.4 The diffusion equation

Using (2.35) and (2.37), the factor $\theta_{1,eq} - \theta_{f,eq}$ becomes

$$\theta_{1,eq} - \theta_{f,eq} = K_0 \exp\left(\frac{q_{st}}{RT}\right) \cdot \Delta p , \tag{2.38}$$

where Δp is the pressure difference across the membrane. From (2.31) and (2.38), a diffusion equation for micropore diffusion can finally be formed:

$$J = \frac{s k_1}{C_{int}} \cdot \frac{d_i}{d} \exp\left(-\frac{E_1}{RT}\right) K_0 \exp\left(\frac{q_{st}}{RT}\right) \Delta p . \tag{2.39}$$

However, in practice it is very difficult to make a good estimation of all the constants in this equation. Since only the temperature dependence of the diffusion is important for the present research, all these factors will be put into a constant D_0, which is characteristic for the microporous material and the diffusing species. With the ideal gas law, $p = nRT$, it follows that for the microporous membrane

$$J = -D\frac{dn}{dz} = -D \cdot \frac{\Delta n}{d} , \tag{2.40}$$

with

$$D = D_0 \cdot T \exp\left(-\frac{E_a}{RT}\right), \tag{2.41}$$

and Δn is the difference in density of mercury atoms in the gas phase across the membrane. The influence of the interface processes, characterized by the factor C_{int}, is neglected. As can be seen from equation (2.30) this is justified, since the jump distance d_j (in the order of 5 Å) is small compared to the thickness of the microporous membrane (in the order of 10 nm). E_a is the apparent activation energy for the diffusion in the membrane[1]:

$$E_a = E_1 - q_{st}. \tag{2.42}$$

It depends on the relative magnitude of E_1 and q_{st} whether E_a is negative or positive.

The factor T is introduced in (2.41) by the transition from a pressure difference to a density difference across the membrane.

In this discussion only the microporous membrane was considered. In practice, this membrane is always on a porous support. If there is no pressure difference across the support, it is sufficient to introduce a temperature independent factor ε in equation (2.41) to account for the porosity of the support. If there is a pressure difference across the support, things become far more complicated. Due to the influence of the substrate, the temperature dependence can be different for different directions of transport. When the temperature dependence of the diffusion coefficient is still described with equation (2.39), this results in a different activation energy E_a for different directions of the transport. This will not be discussed here in detail.

The transport mechanism in the pores depends on the pore size d_p. With micropore diffusion, the strongest temperature dependence can be achieved. The activation energy E_a determines the temperature dependence of micropore diffusion.

The activation energy is changed by changing q_{st} or E_1 in equation (2.42). It is assumed, that the isosteric heat q_{st} can be influenced by introducing so-called "active sites". These are obtained if the microporous material is doped with a metallic material. The activation energy for diffusion, E_1, depends on the pore diameter. As was stated before, the form of the curve of the potential energy (figure 2.1), is due to the Van der Waals forces. Therefore, the potential energy is a function of the distance to the pore wall and thus E_1 is a function of the pore diameter.

---

1. This activation energy can be different from that for surface diffusion, see equation (2.21).

3 EXPERIMENTAL SETUP AND MEASUREMENTS

In table 3.1 the ceramic membranes that are characterized in the experiments described in this report are listed. An experimental setup for absorption measurements is used for the measurement of mercury pressures of amalgams and flow rates through ceramic membranes. First the experimental setup will be discussed, whereafter the measurement of diffusion coefficients will be explained.

Table 3.1 Different types of ceramic membranes used in membrane experiments.

Type of ceramic membrane
α-Al_2O_3
α-Al_2O_3 + γ-Al_2O_3
α-Al_2O_3 + γ-Al_2O_3 + SiO_2 [a]
α-Al_2O_3 + γ-Al_2O_3 + SiO_2

a. This membrane is the standard membrane.

3.1 Experimental setup for mercury pressure measurements

Mercury densities can be measured by a transmission measurement. In such a measurement a lamp emits UV radiation which can be absorbed by mercury. The fraction of radiation that is absorbed in the sample is a measure for the density of mercury atoms in the vapour. In practice, not the absorption but the transmission is measured. This is essentially the experimental setup used for experiments described in this report.

3.1.1 The hardware

Figure 3.1 shows the schematic layout of the experimental setup. The UV lamp providing the radiation that can be absorbed by mercury is on the right. This lamp itself is a mercury lamp, producing 185 and 254 nm UV radiation. The 185 nm radiation is absorbed by the air in the experimental setup. The 254 nm radiation passes through a diaphragm and a lens that focuses the radiation on the head of the optical cuvette. The mercury vapour in the optical cuvette partially absorbs the radiation. The transmitted radiation is finally absorbed in a photodiode. This produces an electric current which is called the transmission signal.

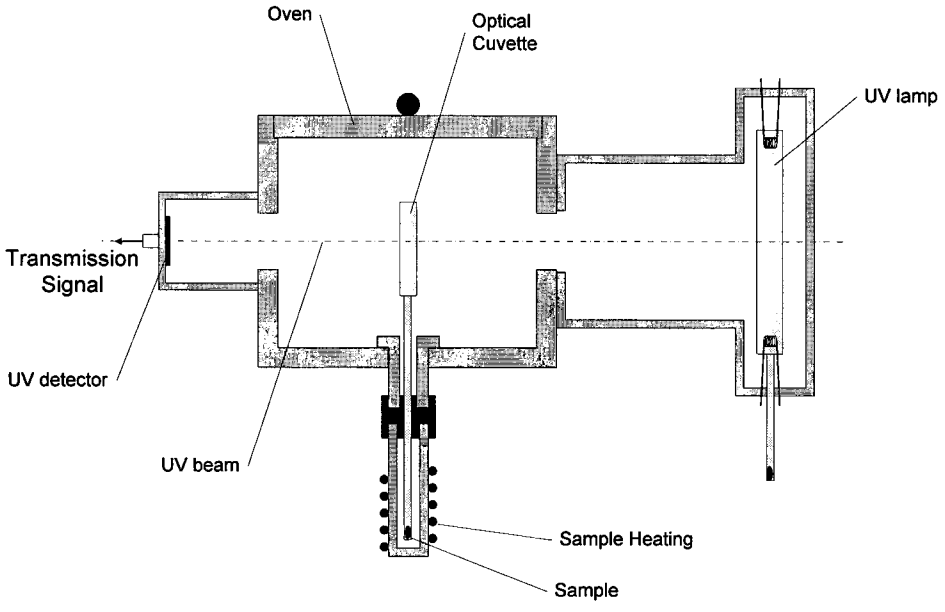

Figure 3.1 Schematic layout of the experimental setup for the measurement of the mercury pressure in an optical cuvette.

The measurements of the temperature and the transmission are automated with a computer. For this automation and further data processing, a computer code using Labview has been developed [13].

3.1.2 Calibration of the experimental setup

The experimental setup is calibrated with a measurement of the transmission as a function of the temperature for a simple mercury sample. For pure mercury, the mercury pressure as a function of temperature is known. This relates a certain transmission to a mercury pressure.

Figure 3.2 shows typical measurements of the relative transmissions of an amalgam sample and a mercury sample (the calibration measurement). The line on the left is the transmission as a function of the temperature as it has been measured in the calibration measurement. The line on the right is the transmission of the amalgam sample as a function of the temperature. The transmission of the amalgam sample at temperature T_a is equal to that measured for the mercury sample at temperature T_{Hg}, so the mercury pressures were equal. The mercury pressure p_{Hg} of mercury at the temperature T_{Hg} is known, so the mercury pressure of the sample at the temperature T_a is determined.

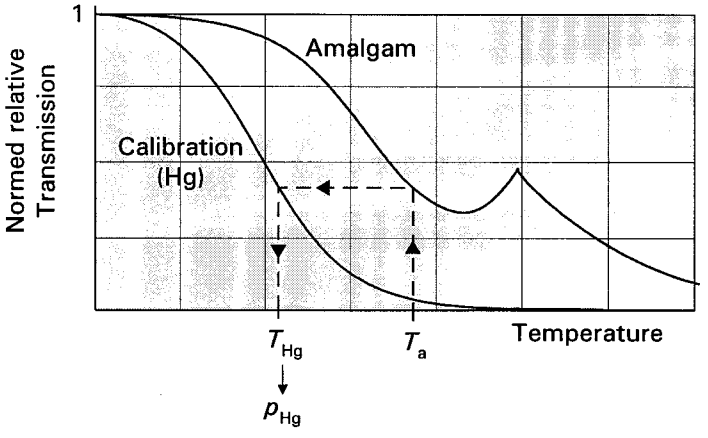

Figure 3.2 Determination of the mercury pressure in the cuvette from the transmission, using a calibration measurement.

3.2 Determination of diffusion coefficients

The flow rate of mercury through ceramic membranes, and thus the diffusion coefficient, can be determined by constantly monitoring the mercury pressure in the cuvette upon a temperature step on the sample. The sample is in a capsule, that is closed with the ceramic membrane under investigation. This is shown schematically in figure 3.3. If the pressure changes, there is a flux from the capsule to the cuvette or reversely. The relevant parameters are the mercury pressure p, the mercury density n in the capsule and in the cuvette (indicated by a subscript cap or cuv) and the temperature T of the system.

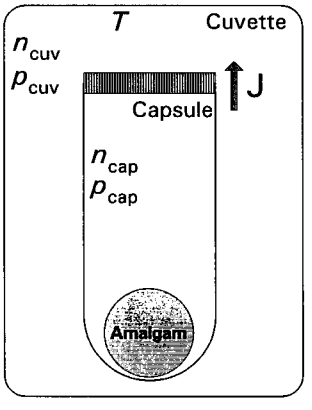

Figure 3.3 Schematic view of the optical cuvette containing a capsule with a ceramic membrane and the most significant parameters involved.

In the derivation of the diffusion coefficients from a given behaviour of the mercury pressure in the cuvette, a few assumptions are made:

- Mercury transport through the ceramic membrane is based on diffusion and thus on a difference in density of mercury atoms across the membrane. Then, equation (2.1)

describes the mercury transport.

- The whole cuvette, the gas in the cuvette and the capsule are all at the same temperature T. This is not true in practice, because the head of the cuvette and the gas in the head are at a constant temperature of 150°C, for reasons mentioned in the previous section. However, the volume of the head is relatively small compared to the volume of the whole cuvette (approximately 0.5 ml in comparison to 3 ml), so this measurement volume is assumed to be negligible.
- The mercury vapours in the cuvette and in the capsule behave like ideal gases: $p = nRT$. This assumption is justified by the fact that the mercury pressures in the capsule and in the cuvette remain much lower than the saturated mercury pressure at the same temperature.
- The amalgam in the mercury capsule will instantaneously control the mercury pressure in the capsule.
- There are no pressure differences within the capsule or within the cuvette (there are effects, like thermal creep and thermal transpiration which can create a minute pressure gradient when there is a temperature gradient [1]. These effects are neglected).

The diffusive flux Φ of mercury atoms through the membrane (mol/s) is given by (see (2.1), (2.40) and (2.41))

$$\Phi = A \cdot J = -D_T \cdot \frac{\mathrm{d}n}{\mathrm{d}z} \cdot A = D_T \cdot \frac{A}{d} (n_{cap} - n_{cuv}) , \qquad (3.1)$$

where A is the surface of the membrane and d is the thickness of the membrane. D_T is the diffusion coefficient at temperature T. D_T is positive, so Φ is defined to be positive for diffusion of mercury into the cuvette ($dN_{cuv}/dt = \Phi$, where N_{cuv} (mol) is the number of mercury atoms in the cuvette).

The sample is given temperature steps from a high temperature T_h to a low temperature T_l and back again. The diffusion coefficients at these temperatures are denoted as D_h and D_l respectively. A typical curve of the mercury pressure in the cuvette as a function of time is given in figure 3.4.

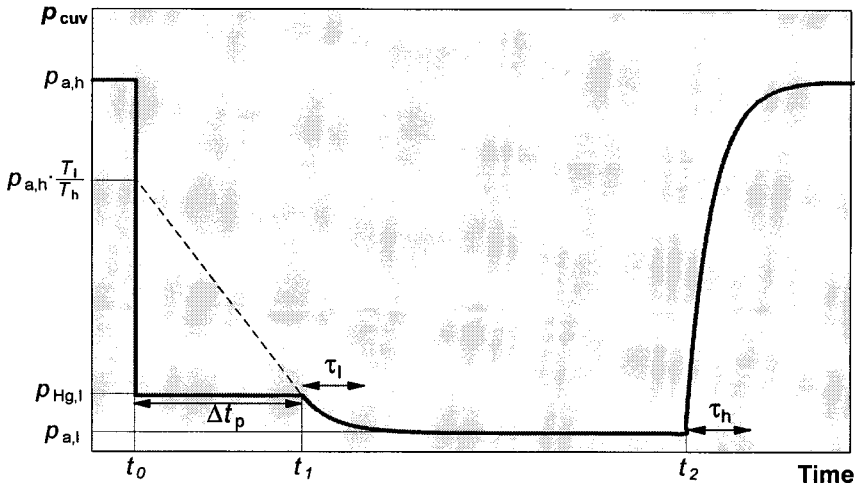

Figure 3.4 Typical curve of the mercury pressure in the cuvette as a function of time. At $t = t_0$ a temperature step from T_h to T_l is made and at $t = t_2$ a step from T_l back again to T_h is given.

When the temperature is high ($T = T_h$) and the mercury pressure in the cuvette has stabilized at $p_{cuv} = p_{a,h}$ (the mercury pressure of the amalgam in the capsule at $T = T_h$), then the number of particles in the cuvette is

$$N_{cuv} = n_{cuv} V_{cuv} = \frac{p_{cuv} V_{cuv}}{RT} = \frac{p_{a,h} V_{cuv}}{RT_h}, \tag{3.2}$$

where V_{cuv} is the volume of the cuvette. When a temperature step from $T = T_h$ to $T = T_l$ is given, the mercury pressure will decrease instantaneously from $p_{a,h}$ to $p_{a,h} \cdot T_l / T_h$. If this pressure is higher than $p_{Hg,l}$, the saturated mercury pressure at $T = T_l$, a little mercury will condensate and a drop of liquid mercury will be formed, forcing the mercury pressure to $p_{Hg,l}$:

$$p_{cuv}(t) = p_{Hg,l} \text{ for } t_0 \le t \le t_1 . \tag{3.3}$$

This is illustrated in figure 3.4. The dotted line represents the mercury pressure in the cuvette as it would be if no drop of liquid mercury was be formed (based on the total number of mercury atoms in the cuvette, not the number of atoms in the gas phase). It is a straight line, because the pressure difference (and with that the concentration gradient) across the membrane is constant and thus the flow rate is constant. Therefore the mercury pressure would decrease linearly. The slope of this line indicates the transport rate. Of course, this slope equals the slope of the mercury pressure in the beginning of the exponential decay at the time t_1.

The amount of mercury in the drop is

$$N_{drop} = N_{cuv} - \frac{p_{Hg,l} V_{cuv}}{RT_l} . \tag{3.4}$$

The rate of mercury absorption by the capsule equals

$$\frac{dN_{cuv}}{dt} = \Phi = D_l \cdot \frac{A}{d}(n_{cap} - n_{cuv}) = D_l \cdot \frac{A}{d} \cdot \frac{p_{a,l} - p_{Hg,l}}{RT_l}, \tag{3.5}$$

where $p_{a,l}$ is the mercury pressure induced by the capsule at $T = T_l$. The time needed to absorb the drop of mercury (the plateau time, $\Delta t_p = t_1 - t_0$) is found by dividing N_{drop} by the transport rate $-dN_{cuv}/dt$:

$$\Delta t_p = \tau_l \cdot \frac{p_{a,h} \cdot \frac{T_l}{T_h} - p_{Hg,l}}{p_{Hg,l} - p_{a,l}}, \tag{3.6}$$

with

$$\tau_l \equiv \frac{V_{cuv}}{D_l} \cdot \frac{d}{A}. \tag{3.7}$$

For $t > t_1$, when all the mercury in the drop is absorbed, or if no drop of liquid mercury was formed at all, n_{cuv} decreases proportionally to the difference in density of mercury particles across the membrane:

$$\frac{dn_{cuv}}{dt} = \frac{1}{V_{cuv}} \cdot \frac{dN_{cuv}}{dt} = \frac{\Phi}{V_{cuv}} = \frac{D_l}{V_{cuv}} \cdot \frac{A}{d}(n_{cap} - n_{cuv}) = \frac{1}{\tau_l} \cdot (n_{cap} - n_{cuv}). \tag{3.8}$$

With the ideal gas law this yields a differential equation for the mercury pressure:

$$\frac{dp_{cuv}}{dt} = \frac{1}{\tau_l}(p_{cap} - p_{cuv}) = \frac{1}{\tau_l}(p_{a,l} - p_{cuv}), \tag{3.9}$$

and with the initial condition $p_{cuv}(t_1) = p_{Hg,l}$ the solution of this equation is:

$$p_{cuv}(t) = (p_{Hg,l} - p_{a,l}) \exp\left(-\frac{t - t_1}{\tau_l}\right) + p_{a,l}, \quad t_1 \le t \le t_2. \tag{3.10}$$

τ_l can be identified with the time constant for the exponential decrease of the mercury pressure in the cuvette at a temperature $T = T_l$.

When the temperature is low ($T = T_l$) and the mercury pressure in the cuvette has stabilized at $p_{cuv} = p_{a,l}$, the density of mercury atoms in the cuvette is:

$$n_{cuv} = \frac{p_{cuv}}{RT} = \frac{p_{a,l}}{RT_l}. \tag{3.11}$$

When a temperature step from $T = T_l$ to $T = T_h$ is given (at $t = t_2$ in figure 3.4) the mercury pressure will increase instantaneously from $p_{a,l}$ to $p_{a,l} \cdot T_h/T_l$. This rise in pressure in usually small since $p_{a,l}$ is small and therefore it will be neglected. After the step the mercury pressure in the capsule is $p_{a,h}$. The density of mercury in the cuvette will now increase proportional to the density difference across the membrane:

$$\frac{n_{cuv}}{t} = \frac{\Phi}{V_{cuv}} = \frac{D_h}{V_{cuv}} \cdot \frac{A}{d}(n_{cap} - n_{cuv}) = \frac{1}{\tau_h} \cdot (n_{cap} - n_{cuv}), \tag{3.12}$$

where

$$\tau_h \equiv \frac{V_{cuv}}{D_h} \cdot \frac{d}{A} \tag{3.13}$$

and D_h is the diffusion coefficient at $T = T_h$. The mercury pressure will satisfy:

$$\frac{dp_{cuv}}{dt} = \frac{1}{\tau_h}(p_{cap} - p_{cuv}) = \frac{1}{\tau_h}(p_{a,h} - p_{cuv}) . \tag{3.14}$$

With the initial condition $p_{cuv}(t_2) = p_{a,l}$ it follows that

$$p_{cuv}(t) = (p_{a,l} - p_{a,h}) \exp\left(-\frac{t - t_2}{\tau_h}\right) + p_{a,h} , \quad t \geq t_2 . \tag{3.15}$$

τ_h can be identified with the time constant for exponential increase of p_{cuv} at a temperature $T = T_h$.

The mercury pressure p_{cuv} is now determined by equations (3.3), (3.10) and (3.15). The time constants τ_l and τ_h can be determined from measurements. Then equations (3.7) and (3.13) give a relation between the time constants τ_l and τ_h and the diffusion coefficients D_l and D_h. However, The surface of the membrane, A, is difficult to measure accurately. Moreover, the second assumption mentioned in the beginning of this section, that the whole cuvette is at the same temperature T, introduces an error. In practice, part of the cuvette is at a temperature of 150°C, which is higher than the temperature in the rest of the cuvette. Therefore, in the previous calculation N_{cuv} is slightly overestimated. To put it differently, the effective volume of the cuvette is a little bit smaller than the real V_{cuv}. Therefore V_{cuv} is also difficult to determine, since the temperature is not known in every part of the cuvette. However, the ratio of the diffusion coefficients D_l and D_h can be determined to a reasonable accuracy. From equations (3.7) and (3.13) it follows that

$$\frac{D_l}{D_h} = \frac{\tau_h}{\tau_l} . \tag{3.16}$$

Besides the ceramic membrane, the amalgam can influence transport rates. The mercury pressures $p_{a,h}$ and $p_{a,l}$ influence Δt_p (equation (3.6)), leaving τ_l constant. The phase structure of the amalgam can have influence too. Some amalgams are solid at room temperature, whereas others still have at least one liquid phase. Amalgams that are solid will not take up mercury very fast, and therefore the amalgam could be the element that limits the mercury take-up instead of the ceramic membrane. In the measurements in this report the $Bi_{70}In_{30}$ 3 wt% Hg amalgam was used. This amalgam has a liquid phase at room temperature, so the mercury take-up is very fast and the ceramic membrane must be the element that limits the transport rate of mercury.

4 RESULTS

4.1 Calibration and amalgam measurements

Calibration measurements were performed for the calibration of the experimental setup. In principle, a calibration measurement will have to be performed only once. However, since the measurement system and the software were changed significantly during the first months of this investigation, a calibration measurement has been carried out at least every month. These measurements were reproducible within the measurement accuracy of approximately 1%. Figure 4.1 shows two typical calibration measurements (mercury pressure as a function of the transmission).

As can be seen, the measurements for different cuvette sizes differ significantly. For a thick cuvette much lower mercury pressures can be measured than for a thin cuvette, because there is more absorption of UV radiation due to the large optical path length. The error is least for pressures of approximately 1 Pa in 1 mm cuvettes and for pressures of approximately 0.1 Pa in 10 mm cuvettes. Mercury pressures below approximately 0.1 Pa are not of interest for the current research. With 1 mm cuvettes, pressures of 0.1 Pa and higher can be measured to enough accuracy, and therefore no further measurements have been performed with different cuvette sizes.

In figure 4.2 a good and a bad calibration measurement are shown. For the bad measurement, the slope of the curve in the graph on the right was non-zero for low temperatures. This is caused by an increase in transmission after normalization. This can happen if there is still liquid mercury in the head of the cuvette at the time of the normalization. In that case, there is transport to the cold spot at the bottom of the cuvette and therefore the mercury density in the head of the cuvette decreases and the transmission increases. In general, if the slope of the curve is non-zero for low temperatures, the calibration measurement failed. However, even if the slopes equals zero, this is no guarantee for a "good" calibration measurement.

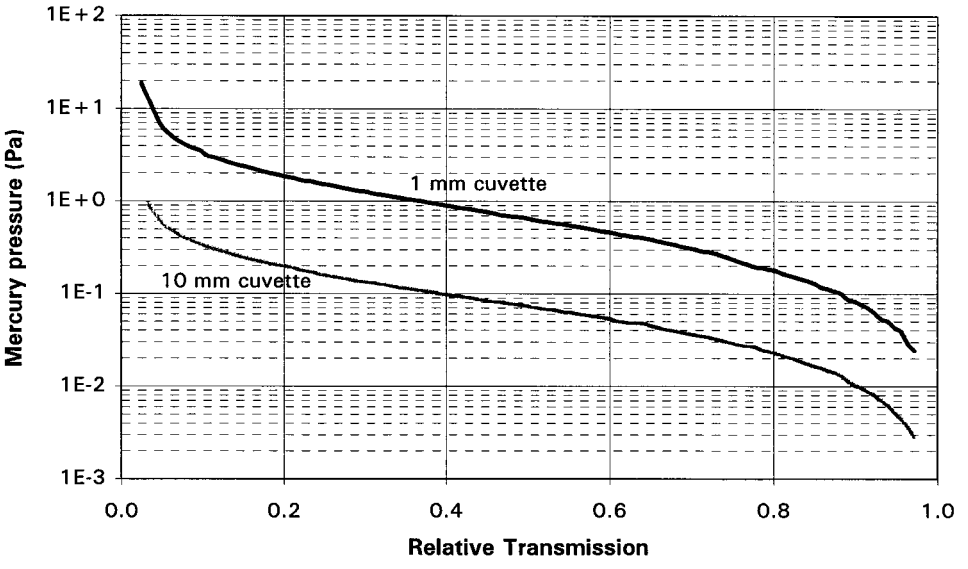

Figure 4.1 Typical calibration measurements for a 1 mm cuvette and a 10 mm cuvette: the mercury pressure calculated from the temperature as a function of transmission.

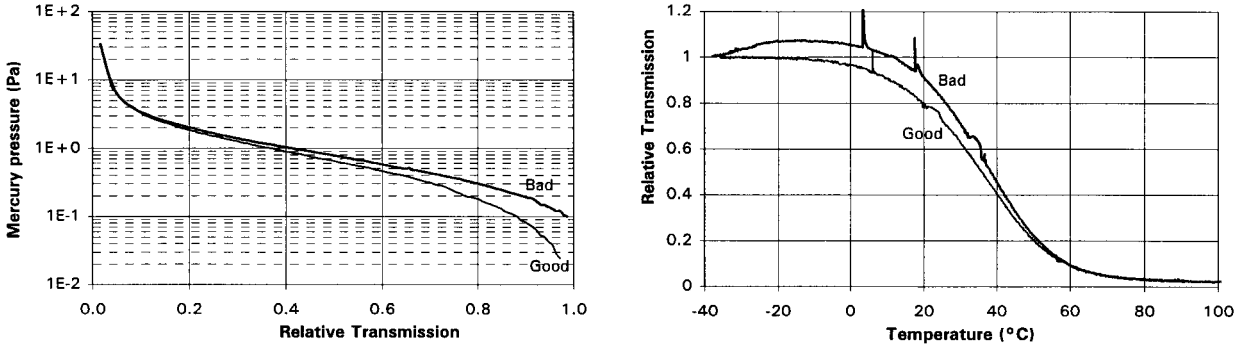

Figure 4.2 A good and a bad calibration measurement. *Left:* the mercury pressure as a function of the transmission, as it can be used directly for amalgam or membrane measurements. *Right:* The normalized relative transmission as a function of the temperature as measured during the calibration measurement.

When a calibration measurement is done, the mercury pressure of amalgams can be measured as a function of the temperature. A typical amalgam curve is shown in figure 4.3.

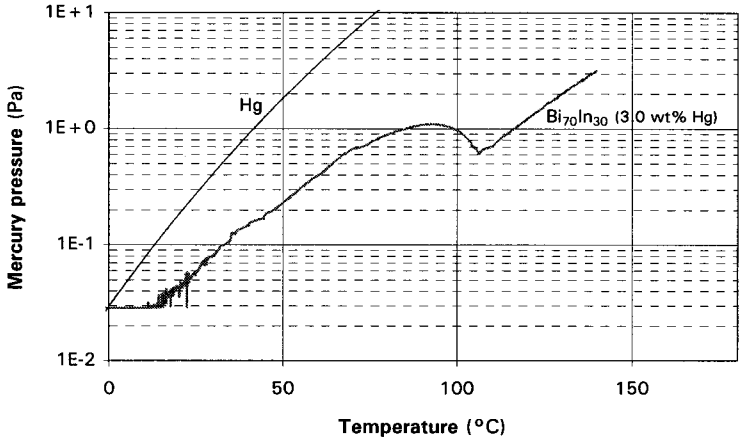

Figure 4.3 The mercury pressure of the $Bi_{70}In_{30}$ 3 wt% Hg amalgam as a function of the amalgam temperature.

A difference in mercury pressure can be found between measurements with increasing and decreasing temperatures. This difference is due to the supercooling effect. The measurement in figure 4.3 is measured with increasing temperature. However, with decreasing temperature, the straight line on the right continues until temperatures below 106°C. An illustration of this supercooling effect is shown in figure 4.4. For temperatures higher than 106°C, the amalgam is completely liquid and for lower temperatures there are solid phases (assumed that the amalgam is in thermodynamical equilibrium). If the temperature decreases, the amalgam can remain completely liquid, even for temperatures below 106°C. This causes the lower mercury pressure. If the temperature is decreased further, the amalgam suddenly becomes solid and the mercury pressure increases.

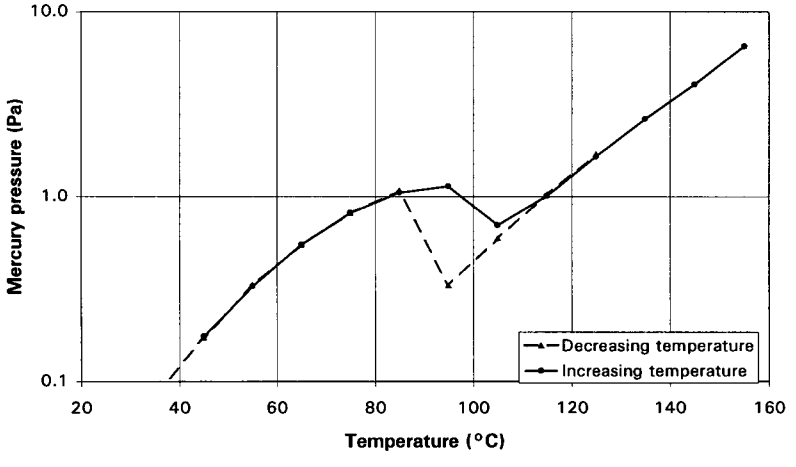

Figure 4.4 The mercury pressure of $Bi_{70}In_{30}$ 3 wt% Hg measured for increasing temperature and for decreasing temperature. The supercooling effect is clearly visible.

4.2 Measurements on ceramic membranes

The amalgams used for membrane measurements are $Pb_{20}Bi_{46}Sn_{34}$ 3 wt% Hg and $Bi_{70}In_{30}$ 3 wt% Hg. Both amalgams have a mercury pressure that is at a maximum (approximately 1.2 Pa) at temperatures of 82°C and 92°C respectively. The PbBiSn amalgam is used only in experiments on the capsule with a macroporous α-Al_2O_3 membrane. Measurements on capsules with the other ceramic membranes (listed in chapter 3) are performed with the Biln amalgam. It is preferable to use the Biln amalgam, since this amalgam has a liquid phase at room temperature and will therefore take up or evaporate mercury very quickly (see at the end of section 3.2).

4.2.1 Verification of the measurement technique

In figure 4.5 a measurement on a standard capsule (with a SiO_2 membrane, placed on the inner side of the capsule) is shown. The thin line is the measured mercury pressure, and the thicker line is the mercury pressure according to the model described in chapter 3. Here, mercury pressures, time constants and the plateau time are used as fitting parameters.

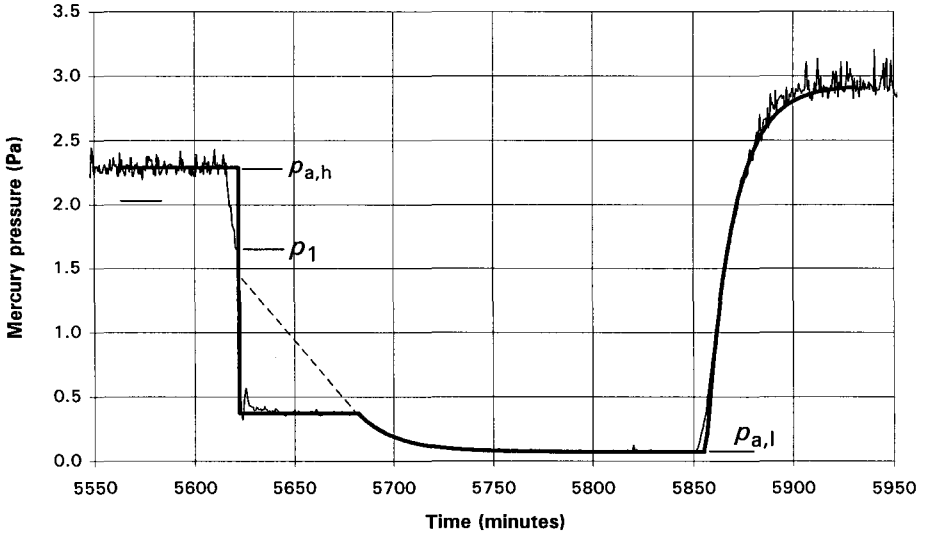

Figure 4.5 A membrane measurement on a capsule with a standard membrane. The dotted line is comparable to that in figure 3.4. The temperature is initially 130°C and decreases to 35°C in the time $t = 5619$ to $t = 5622$. A temperature step to 135°C is made at $t = 5855$. The time constants are $\tau_{35} = 19$ min. and $\tau_{135} = 14$ min., and the plateau time is $\Delta t_p = 60$ min.

In figure 4.5 it can clearly be seen that when the temperature starts to decrease (at $t = 5619$ min.), the mercury pressure also begins to decrease. Firstly, the pressure decreases from the equilibrium amalgam pressure at high temperature, $p_{a,h}$, to the pressure $p_1 = p_{a,h} \cdot T_l / T_h$. This is the pressure fall as a direct consequence of the temperature decrease (ideal gas law), as argued in section 3.2. For the present measurement $p_1 = 1.75$

Pa. After this decrease, at $t=5622$, there is a very sharp decrease in mercury pressure due to condensation of mercury. The mercury pressure becomes equal to $p_{Hg,l}$, the mercury pressure of mercury at $T=35°C$.

There are a few deviations from the model described in section 3.2. The first (small) deviation is the deviation in the mercury pressure at the moment that the sharp decrease in mercury pressure begins. According to the discussion above, this should be $p_1 = 1.75$ Pa. In practice, however, the measured pressure is 1.65 Pa. This small difference is due to the fact that the temperature step is not ideal. During the decrease of the mercury pressure from $p_{a,h}$ to p_1, the capsule already absorbs a little mercury. Therefore, the pressure will decrease more than predicted by the model (note that according to the model the pressure decrease from $p_{a,h}$ to p_1 is not visible in the first place). This effect also occurs at the positive temperature step at $t=5855$.

The second deviation, which is more important, is a deviation in the plateau time. The plateau time is 60 minutes in the measurement shown in figure 4.5. However, from equation (3.6) the plateau time is expected to be 86 minutes for the measured time constant $\tau_{35} = 19$ min. Again, the reason for this is that the temperature step is not ideal. The plateau time is proportional to the number of particles in the drop of liquid mercury that arises when the temperature is suddenly lowered. The pressure difference across the membrane is $p_{Hg,l} - p_{a,l}$. This difference strongly increases for increasing temperature. Therefore, the transport rate is also much higher for higher temperatures (even for a constant diffusivity) and thus the plateau time strongly decreases if the temperature is slightly too high. During the temperature step, the temperature is higher than 35°C, which causes the short plateau time. Moreover, a small temperature fluctuation in the temperature after the step will also affect the plateau time strongly. Since the plateau time is too short, the dotted line in figure 4.5 does not match the pressure p_1 at the time $t=5622$.

A measurement for which the plateau time matches the time constant at low temperature is shown in figure 4.6. In this figure a logarithmic scale is used. The plateau time measured is 93 minutes, whereas the plateau time that is expected for $\tau_{25} = 27$ min. is 92 minutes. Here the plateau time is also shortened by the non-ideality of the temperature step, but accidentally the temperature is too low for some time, which increases the plateau time. Therefore, it is purely coincidence that the plateau time and time constant match in this case.

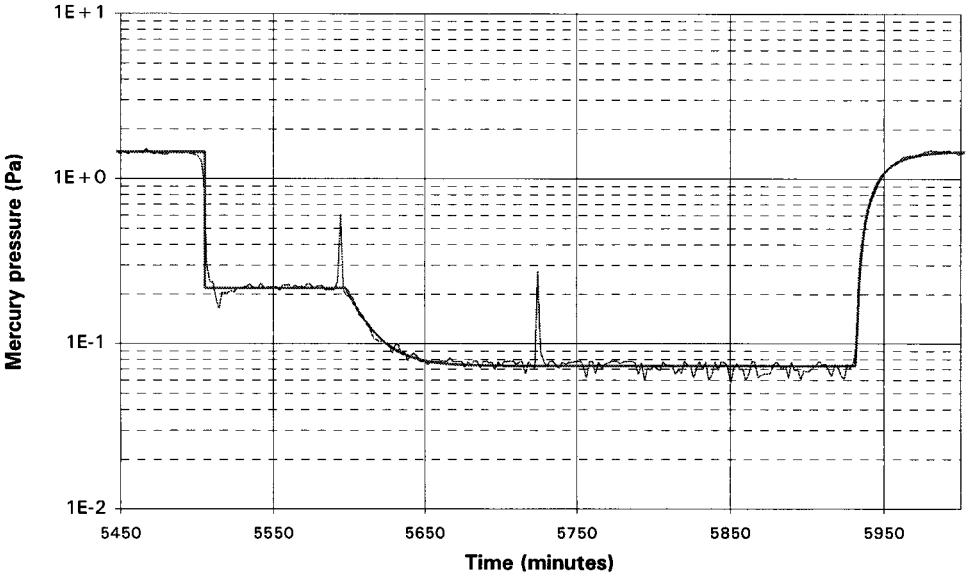

Figure 4.6 Membrane measurement on a capsule with only the support α-Al_2O_3 membrane. The temperature starts at 95 °C and decreases to 25 °C at $t = 5505$. At $t = 5932$ the temperature increases to 95 °C. The plateau time is $\Delta t_p = 93$ min. and the time constants are $\tau_{25} = 17$ min. and $\tau_{95} = 14$ min. The sharp peaks in the signal are noise, caused by the photo amplifier.

A third deviation from the model described in chapter 3 is the mercury pressure at the plateau. This should be equal to the saturated mercury pressure at the low temperature. However, in almost every measurement the mercury pressure at the plateau (p_{pl}) is lower. In figure 4.5 $p_{pl} = 0.37$ Pa where $p_{Hg,l} = 0.74$ Pa, and in figure 4.6 $p_{pl} = 0.22$ Pa where $p_{Hg,l} = 0.33$ Pa. The most probable explanation for this difference is that the temperature of the coldest spot in the cuvette is lower than the temperature measured by the thermocouple. The end of the cuvette is further from the electrical heating than the thermocouple (see figure 4.7) and could therefore be colder. A temperature difference of approximately 5 degrees is enough to explain the measured pressure difference.

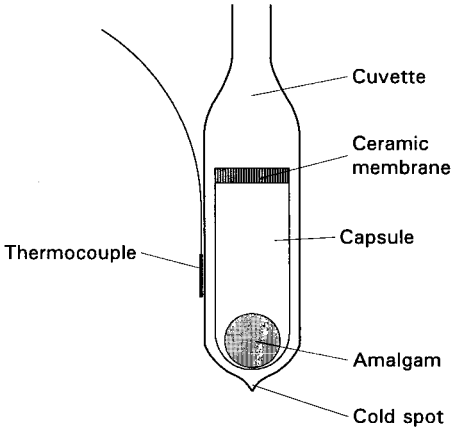

Figure 4.7 The lower part of the optical cuvette in the experimental setup.

Although there are some small deviations from the model developed in chapter 3, it can be assumed to be a reliable model, because most differences measured can be explained easily. Therefore, the time constants that are measured are assumed to be inversely proportional to the diffusion coefficients (see equations (3.7) and (3.13)). However, there are measurements in which there are still unexplained deviations. An example of such a measurement is shown in figure 4.8. It seems that there is a second exponential in the curve for decreasing pressure. The first exponential is taken into account in membrane measurements, since in that case the results are most reproducible. However, effects like these can decrease the accuracy of the time constants. Therefore, the ratios of diffusion coefficients are not determined to great accuracy in most cases.

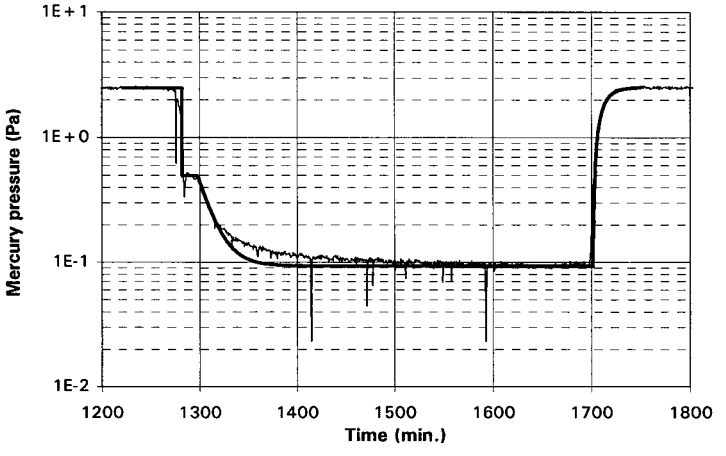

Figure 4.8 The mercury pressure as a function of the time in a measurement on a γ-Al_2O_3 ceramic membrane. When the mercury pressure decreases, it follows an exponential (indicated by the thicker line), but for $t > 1320$ minutes, a different exponential is followed. This is a deviation from the model that is thus far unexplained.

4.2.2 Transport types, transport rates and activation energies

Measurements on the α-Al_2O_3 ceramic membranes

Measurements on the α-Al_2O_3 ceramic membranes are done with the $Pb_{20}Bi_{46}Sn_{34}$ 3 wt% Hg amalgam. The temperatures that are used in these membrane measurements are 25°C and 95°C. The measured time constants for these temperatures and the resulting ratios of diffusion coefficients D_{95}/D_{25} (see equation (3.16)) are listed in table 4.1. It can be seen that there is a relatively large uncertainty in the measurements, because of the unexplained deviations from the model, mentioned in the previous section. The uncertainty has been estimated from the exponential fit.

For Knudsen diffusion, the ratio of diffusion coefficients at these temperatures is (see equation (2.16)):

$$\frac{D_{95}}{D_{25}} = \sqrt{\frac{368}{298}} = 1.11 .$$

The ratios of diffusion coefficients listed in table 4.1 equal this value within the measurement uncertainty, so it can be assumed that the transport mechanism is Knudsen diffusion. However, for Poiseuille flow the temperature dependence is also $T^{1/2}$. Therefore no prediction of the transport mechanism (either Poiseuille flow or Knudsen diffusion) can be made from these measurements.

Table 4.1 The averaged time constants at the temperatures $T = 25\,°C$ and $T = 95\,°C$ and the ratios of diffusion coefficients at these temperatures for the macroporous α-Al_2O_3 membrane.

Capsule number	$\langle\tau_{25}\rangle$	$\langle\tau_{95}\rangle$	$\langle D_{95}/D_{25}\rangle$
1	12 ± 2	11 ± 2	1.09 ± 0.4
2	17 ± 2	14 ± 2	1.21 ± 0.3
3	23 ± 5	17 ± 3	1.35 ± 0.5

The Knudsen number can however make a theoretical prediction of the transport mechanism. The Knudsen number can be calculated according to (2.4):

$$\mathrm{Kn} \equiv \frac{\lambda}{d_p}.$$

The optical cuvettes are filled with 400 Pa argon filling gas at a temperature $T = 298$ K. The mercury pressure (in the order of 1 Pa) barely contributes to the total pressure. The mean free path length is then given by (2.11): $\lambda \approx 14$ µm. The pore sizes in the macroporous α-Al_2O_3 membrane are approximately $d_p \approx 30$ nm. Then the Knudsen number is $\mathrm{Kn} \approx 5 \cdot 10^2 \gg 1$. It may therefore be assumed that the transport mechanism in the macroporous α-Al_2O_3 membrane is indeed Knudsen diffusion.

Measurements on mesoporous γ-Al_2O_3 membranes

Only one measurement on a mesoporous γ-Al_2O_3 membrane has been performed. This capsule had the γ-Al_2O_3 layer on the inner side. The amalgam used in this experiment is the $Bi_{70}In_{30}$ 3 wt% Hg amalgam and the temperatures used are 35°C and 135°C. The average time constants and ratio of the diffusion coefficients are listed in table 4.1.

Table 4.2 The averaged time constants at the temperatures $T = 35\,°C$ and $T = 135\,°C$ and the ratio of diffusion coefficients at these temperatures for the mesoporous γ-Al_2O_3 membrane.

Capsule number	$\langle\tau_{35}\rangle$	$\langle\tau_{135}\rangle$	$\langle D_{135}/D_{35}\rangle$
1	12.3 ± 2	12.1 ± 1	1.02 ± 0.3

The time constants measured in this experiment are in the same order of magnitude as the time constants measured for the macroporous α-Al_2O_3 membranes (see table 4.1). However, the surface of the α-Al_2O_3 membranes is only approximately 2 mm^2, whereas the surface of the mesoporous γ-Al_2O_3 membrane is approximately 20 mm^2. Thus the diffusion coefficient in the γ-Al_2O_3 membrane is approximately 10 times lower than in the

α-Al_2O_3 membrane (see equations (3.7) and (3.13)).

The ratio of the diffusion coefficients at 135°C and 35°C, expected for Knudsen diffusion, is

$$\frac{D_{135}}{D_{35}} = \sqrt{\frac{408}{308}} = 1.15 .$$

The ratio of diffusion coefficients measured in this experiment is thus within measurement uncertainty of this value.

The average pore diameter of these membranes is in the order of 10 nm. Therefore the Knudsen number is approximately $Kn \approx 1.5 \cdot 10^3$, even larger than in the α-Al_2O_3 support. Then Poiseuille flow does not play a significant role. Furthermore, the classical diameter of a mercury atom is approximately 0.7 nm, which is much smaller than the average pore diameter (approximately 10 nm). Therefore, surface diffusion is not expected to play a significant role either in the mercury transport. Thus Knudsen diffusion is expected to be the most important transport mechanism for γ-Al_2O_3 membranes. This is affirmed by the measurement on this membrane.

Measurements on the microporous SiO_2 membranes

It is expected that for microporous SiO_2 membranes the diffusion coefficient depends on the direction of transport, that is, whether the transport is from the SiO_2 membrane to the α-Al_2O_3 support or reversely. In an ordinary membrane experiment, however, the transport at high temperature (135°C) and the transport at low temperatures (35°C) are in opposite directions. Therefore the transport rates for these temperatures cannot be compared directly. In order to study the temperature dependence of the transport the time constants for the transport have been determined as a function of the temperature. In these measurements either positive or negative temperature steps of 10°C are given. Then the direction of the transport is the same for several temperature steps and the measured time constants can be compared.

For increasing temperature, the mercury pressure of the amalgam generally increases. Therefore, the transport is directed outward of the capsule for positive temperature steps: the feed side of the membrane is on the inner side of the capsule (see figure 4.9).

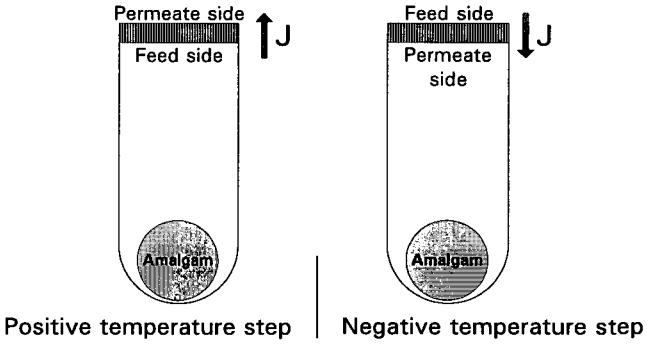

Figure 4.9 Definition of the feed side of the membrane. The transport is directed from the feed side of the membrane to the permeate side.

In figure 4.10 the temperature dependence of the time constants measured for transport through a SiO_2 membrane on the inner side of the capsule is shown for positive and negative temperature steps. The SiO_2 membrane is thus on the feed and permeate side respectively. Since $\tau \sim 1/D$ and $D = D_0 T \exp(-E_a/RT)$ [1], the time constant τ is of the form

$$\tau = \left[C \cdot T \cdot \exp\left(-\frac{E_a}{RT}\right) \right]^{-1},$$

where C is proportional to D_0. This function has been fitted to the measured values of τ. The resulting activation energies E_a (J/mol) and proportionality constants C ($K^{-1}s^{-1}$) are listed in table 4.3.

In figure 4.11 a measurement of the time constants measured for transport through a SiO_2 membrane on the outer side of the capsule is shown. The corresponding activation energies E_a and proportionality constants C are listed in table 4.4.

1. The diffusion mechanism is not Knudsen diffusion or Poiseuille flow, since the temperature dependence of the transport is negative (an increased temperature leads to a decrease in diffusion coefficient).

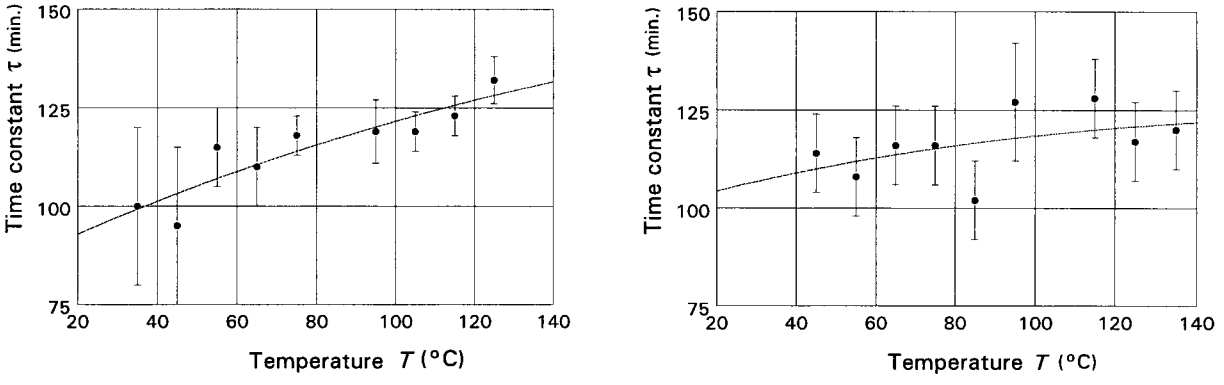

Figure 4.10 The time constants measured for transport through the SiO_2 membrane capsule, with the silica layer on the inner side. *Left:* transport with the SiO_2 layer on the permeate side (negative temperature steps). *Right:* transport with the SiO_2 layer on the feed side (positive temperature steps).

Table 4.3 Activation energies E_a and proportionality constants C for the measurement on the SiO_2 membrane capsule with the silica layer on the inner side.

feed side	E_a (kJ/mol)	C ($\cdot 10^{-6}$ $K^{-1}s^{-1}$)
α-Al_2O_3	-5.8	3.4
SiO_2	-4.2	5.9

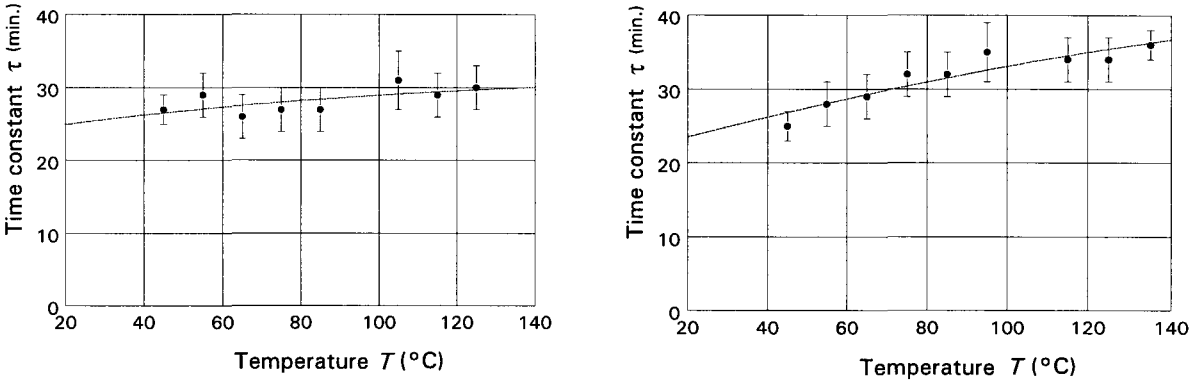

Figure 4.11 The time constants measured for transport through the SiO_2 membrane capsule with the silica layer on the outer side. *Left:* transport with the SiO_2 layer on the feed side (negative temperature steps). *Right:* transport with the SiO_2 layer on the permeate side (positive temperature steps).

Table 4.4 Activation energies E_a and proportionality constants C for the measurement on the SiO_2 membrane capsule with the silica layer on the outer side.

feed side	E_a (kJ/mol)	C ($\cdot 10^{-6}$ $K^{-1}s^{-1}$)
α-Al_2O_3	-6.6	9.7
SiO_2	-4.4	22

From the measurements described here, it can thus be concluded that if the microporous silica layer is on the feed side, $|E_a|$ is on the average a factor 1.44 lower and C is on the average a factor 2.0 higher than when the α-Al_2O_3 support is on the feed side. Thus when the silica layer is on the feed side, the temperature dependence due to the activated transport is weaker and the transport rate is higher.

Also, a few "normal" membrane measurements on these membranes were performed. The time constants measured in these experiments are listed in table 4.5. For the capsule with the SiO_2 layer on the inner side, $\langle\tau_l\rangle$ can be compared with the time constant for $T = 35\,°C$ in the graph on the left in figure 4.10. It can be seen that the time constants τ_h measured in the normal membrane measurement match the time constants measured in the experiments described above, but the time constants τ_l do not match within measurement uncertainty. This could be due to the larger temperature steps that are made in the normal membrane measurements.

Table 4.5 Time constants for the transport through SiO_2 membranes in "normal" membrane measurements.

	$\langle\tau_l\rangle$	$\langle\tau_h\rangle$
SiO_2 inner side	114 ± 5 (see figure 4.10, left)	123 ± 5 (see figure 4.10, right)
SiO_2 outer side	32 ± 3 (see figure 4.11, left)	32.5 ± 3 (see figure 4.11, right)

4.2.3 Concluding remarks

A few general remarks about the membrane measurements can be made.

- There are still some unexplained deviations from the model for the behaviour of the mercury pressure in a cuvette with a capsule. One of these is the "second exponential", illustrated in figure 4.8. These effects can make it difficult to fit an exponential function through the measured datapoints and thus they increase the measurement uncertainty.

- If the difference between the temperature dependencies of Knudsen diffusion and activated transport is large, this can certainly be seen in the measurements. Since this is not the case, it is very difficult to make predictions about the transport mechanism, because of the relative large uncertainty in the measurements. In the measurements presented in the previous section, the difference between Knudsen diffusion and activated transport can be made because of the negative temperature dependence of the transport.

- The measurements can probably be done with a much greater accuracy if the diffusion coefficient is measured for much broader temperature ranges. However, the experimental setup used for this study is not suitable for temperatures higher than roughly 150°C. Much lower temperatures cannot be used either, since mercury solidifies at -39°C. Moreover, the range of mercury pressures that can be measured is limited by the cuvette size (roughly 0.2 to 4 Pa with a 1 mm cuvette).

5 CONCLUSIONS

The following conclusions can be drawn from this investigation:

- Absolute mercury pressure measurements can be done to an accuracy of 20% for mercury pressures between 0.2 and 4 Pa when a 1 mm cuvette is used. When a 10 mm cuvette is used, mercury pressures between 0.02 and 0.4 Pa can be measured to an accuracy of 20%. Mercury pressure measurements are reproducible to a greater accuracy (approximately 10-15%), since the errors are partially systematic.

- It is preferable for membrane measurements, to use an amalgam that has a liquid phase at room temperature, like $Bi_{70}In_{30}$ 3 wt% Hg, because of the fast transport of mercury within an amalgam that has a liquid phase.

- The technique for membrane measurements that was used in this investigation works very well. There are a few deviations, for example the plateau time Δt_p does not match the time constant τ_l in most cases, but these will not influence the results. However, in a few measurements systematic deviations from this model occur. These have not yet been explained.

- The transport mechanism of mercury through macroporous α-Al_2O_3 membranes is expected to be Knudsen diffusion ($Kn \approx 5 \cdot 10^2 \gg 1$). The temperature dependence of the diffusivity, measured in membrane measurements, equals the temperature dependence that is expected for Knudsen diffusion within the measurement uncertainty. However, the temperature dependence of Poiseuille flow is the same as for Knudsen diffusion. Therefore Poiseuille flow is not excluded by the measurements.

- The transport rate of mercury through mesoporous γ-Al_2O_3 membranes is approximately 10 times smaller than the transport rate through macroporous α-Al_2O_3 membranes. The most important transport mechanism is still Knudsen diffusion.

- The diffusion of mercury through the microporous silica membranes is activated. The activation energies range from -6.6 to -4.2 kJ/mol. The fact that the activation energy is negative, leads to a negative temperature dependence.

- The activation energy and the transport rate in the microporous membrane depend on the direction of the mercury flow. When the silica layer on the membrane is on the feed side, the transport rate is higher. The absolute value of the activation energy is lower, thus the temperature dependence of the transport due to activated transport

is weaker.

- For measurements on the SiO_2 membranes, there is a difference of up to approximately 20% between time constants measured in normal membrane measurements and the time constants measured in membrane measurements in which only small temperature steps are given. The reason for this deviation is not known.

REFERENCES

[1] Arney G.D.jr., Kinslow M., *Thermo-Molecular Pressure Effects in Tubes and Orifices*, AGARDograph 119 (1967)

[2] Atkins P.W., *Physical chemistry*, Oxford University Press, third edition (1986)

[3] Barrer R.M., *Porous Crystal Membranes*, J. Chem. Soc. Faraday Trans., 86(7) (1990), p.1123-1130

[4] Beijerinck H.C.W., *Collegedictaat Thermische Verschijnselen*, Collegedictaat 3311, Eindhoven University of Technology (1992), p.68-78

[5] Bloem J., Bouwknegt A., Wesselink G.A., *Amalgamen voor TL-lampen*, Philips techn. T. 38 1978/79 no.1, p. 12-17

[6] Burggraaf A.J.,Keizer K., Lange R.S.A. de, *Analysis and theory of gas transport in microporous sol-gel derived ceramic membranes*, Journal of Membrane Science 104 (1995), p.81-100

[7] Burggraaf A.J., Keizer K., Leenaars A.F.M., *Scheiding m.b.v. anorganische membranen*, University of Twente, internal report CT82/157/135 (1982)

[8] Deusing P.H.J., *Analytical models for gas transport through porous membranes*, University of Twente, internal report CT96\639\31 (1996)

[9] Gaarden, H.W. van der, *Amplifier for Photocel UV photometer*, Philips Lighting internal report DRD 2026/95 (1995)

[10] *Gmelins Handbuch der anorganischen Chemie, Quecksilber, lieferung A.1.*, Verlag Chemie, GMBH., Weinheim/Bergstrasse (1960), p.345-351

[11] Kärger J., Ruthven D.M., *Diffusion in zeolites and other microporous materials*, John Wiley and Sons, New York (1992)

[12] Nijmeijer A., *Gas transport through porous materials*, University of Twente, internal report CT96\194\31 (1996)

[13] Sande M.J.v.d., *Handleiding voor kwik dampdrukmetingen met Labview*, Philips Lighting internal memo LAMPS I 030/97

[14] Venema M.K., *Irreversible thermodynamic models for gas transport through porous membranes*, University of Twente, internal report CT96\724\31 (1996)

[15] Vossers G., *Fysische transportverschijnselen voor W.*, Collegedictaat 3438, Eindhoven University of Technology (1986)

[16] Vroon Z.A.E.P., *Synthesis and Transport studies of thin Ceramic Supported Zeolite (MFI) Membranes*, Ph.D. thesis, University of Twente (1995)

[17] Zwegers M. *Static and dynamic mercury vapour pressure measurements*, Trainee report LAMPS I 4005/96 (1996)

LIST OF SYMBOLS

Latin symbols

A	$[m^2]$	*Surface of a membrane*
C_{int}	[-]	*Correction factor on the micropore diffusivity due to interface processes*
d	[m]	*Thickness of a membrane*
d_p	[m]	*Average pore diameter*
d_j	[m]	*Jump distance in a micropore (distance between adsorption sites)*
D	$[m^2/s]$	*Diffusion coefficient (generally used in Fick's law)*
D_K	$[m^2/s]$	*Diffusion coefficient for Knudsen diffusion*
D_P	$[m^2/s]$	*Diffusion coefficient for Poiseuille flow*
D_s	$[m^2/s]$	*Diffusion coefficient for surface diffusion*
E_1	[J/mol]	*Activation energy for intracrystaline diffusion*
E_a	[J/mol]	*Apparent activation energy for micropore diffusion (and surface diffusion)*
f	[-]	*Number of sites in a micropore*
J	$[mol/m^2s]$	*Flux of gas atoms or molecules per unit of surface area*
J_{id}	$[mol/m^2s]$	*Flux of gas atoms per unit area due to micropore diffusion only*
j_s	[mol/ms]	*Flux of gas atoms on a surface per unit length (surface diffusion)*
J_s	$[mol/m^2s]$	*Flux of gas atoms in a porous material due to surface diffusion*
Kn	[-]	*The Knudsen number*
M	[kg/mol]	*Molecular weigth*
n	$[mol/m^3]$	*Density of (mercury) atoms*
N	[mol]	*Number of mercury atoms*
p	[Pa]	*Mercury vapour pressure*
q	$[mol/m^2]$	*Concentration of atoms adsorbed on a surface*
q_s	$[mol/m^2]$	*Saturated concentration of atoms adsorbed on a surface*
q_{st}	[J/mol]	*Isosteric heat of adsorption*
R	[J/molK]	*Universal gas constant (=8.31 J/molK)*
Re	[-]	*The Reynolds number*
s	$[m^{-2}]$	*The number of pores per unit area*
T	[K]	*Temperature*
v	[m/s]	*Mean velocity of gas atoms*
V_{cuv}	$[m^3]$	*Volume of the optical cuvette*

Greek symbols

ε	[-]	*Porosity of a membrane*
η	$[Ns/m^2]$	*Viscosity of a gas*

Θ_K	*[-]*	*Reflection coefficient of the pore wall for Knudsen diffusion*
θ	*[-]*	*Occupation degree*
Φ	*[mol/s]*	*Flux through a porous membrane ($\Phi = A \cdot J$)*
λ	*[m]*	*Mean free path length*
ρ	*[kg/m^3]*	*Mass density of a material or of a gas*
σ	*[m]*	*Only in the combination $\pi\sigma^2$, being the cross section for collisions*
τ	*[-]*	*Tortuosity of the pores in a membrane (Chapter 2);*
		Time constant for mercury pressure change (Chapter 3)

Commonly used subscripts

a	*of an amalgam*
Hg	*of pure mercury*
cuv	*in the cuvette*
cap	*in the capsule*
eq	*in equilibrium*
h	*at a temperature T_h*
l	*at a temperature T_l*
T	*at a temperature T (for diffusion coefficients; sometimes T is replaced by a number, always representing a temperature in °C).*

ACKNOWLEDGMENTS

This report would not have been written but for the help and patience of a few people. In particular, I would like to thank Martin van de Ven for his time and numerous suggestions for the improvement of this report. Furthermore I am grateful to Hans van Haastrecht, Wil van de Bogert, Corine Staats and all other colleagues for their support and pleasant cooperation during my research at Philips Lighting. Volker Hildenbrand and Arian Nijmeijer have been a great help in understanding the chemical theories about micropore diffusion and physisorption. At the Eindhoven University of Technology, I would like to thank Frits de Hoog and Gerrit Kroesen for their patience and contributions. Finally, I would like to thank all people in my direct environment, and Marianne Seibert in particular, for the patience they showed during the last few months of my study.